Synthesis and Characterization of Novel Linear PB-*b*-PS-*b*-PEO and PE-*b*-PS-*b*-PEO Triblock Terpolymers

Adriana Boschetti-de-Fierro,[†] Alejandro J. Müller,[‡] and Volker Abetz*,[†]

Institute of Polymer Research, GKSS Research Centre Geesthacht GmbH, 21502 Geesthacht, Germany, and Grupo de Polímeros USB, Departamento de Ciencia de los Materiales, Universidad Simón Bolívar, Apartado 89000, Caracas 1080-A, Venezuela

Received November 7, 2006; Revised Manuscript Received December 7, 2006

ABSTRACT: Novel polybutadiene-*block*-polystyrene-*block*-poly(ethylene oxide) (PB-*b*-PS-*b*-PEO) linear triblock terpolymers have been synthesized by sequential living anionic polymerization. Further catalytic hydrogenation led to polyethylene-*block*-polystyrene-*block*-poly(ethylene oxide) (PE-*b*-PS-*b*-PEO), a triblock terpolymer with two crystallizable blocks and a glassy middle block. Bulk morphologies have been studied by transmission electron microscopy (TEM) and small-angle X-ray scattering (SAXS) for different compositions. Thermal properties of the PEO block, as determined by differential scanning calorimetry (DSC), showed dependence with the block volume fraction (ϕ_{PEO}) and its polymerization degree (N_{PEO}). The corresponding properties for the PE block are also functions of the polymerization degree (N_{PE}) and the volume fraction of the PEO block (ϕ_{PEO}). Since the PEO block is the first to segregate from solution in toluene, its volume fraction determines the overall morphology and consequently the thermal properties of the studied terpolymers.

Introduction

Block copolymers constitute an intensively studied field due to their ability of self-assembly into ordered microphases in case the blocks are incompatible.[1] The polymer−polymer interaction will generally drive the separation into microphases according to the volume fractions of the different blocks. If other processes come into play, such as crystallization, then the microphase separation from the homogeneous melt will compete with the development of crystals. Therefore, crystallization can occur within the microdomains and be confined into a given geometry (spheres, cylinders, lamellae), or it can overcome the previously generated microphases and undergo the so-called break-out crystallization.[2,3]

The morphology of diblock copolymers with one crystallizable block has already been studied for polybutadiene-*block*-poly(ethylene oxide),[4,5] polystyrene-*block*-poly(ethylene oxide),[6−9] and polystyrene-*block*-polyethylene,[10−12] among many others,[2,13] where confined crystallization was observed and the melt morphology was preserved.

An even more complicated situation is given by increasing the number of crystallizable blocks within diblock copolymers or triblock terpolymers with two crystalline blocks. In those cases the morphology generation is now in competition with two crystallization processes, and the crystallization of the block crystallizing at lower temperature can be either enhanced or disturbed by the already crystallized block. Some examples are the studies of poly(ϵ-caprolactone)-*block*-poly(ethylene oxide),[14,15] poly(*p*-dioxanone)-*block*-poly(ϵ-caprolactone),[16−18] polyethylene-*block*-poly(ethylene oxide),[19] poly(L-lactide)-*block*-poly(ϵ-caprolactone),[20,21] polystyrene-*block*-poly(ethylene oxide)-*block*-poly(ϵ-caprolactone),[22] and polystyrene-*block*-polyethylene-*block*-poly(ϵ-caprolactone).[23−25] The crystallization of diblock copolymers and terpolymers with more than one crystallizable block has been the subject of a recent review.[26]

In this contribution the synthesis of novel polybutadiene-*block*-polystyrene-*block*-poly(ethylene oxide)s with different compositions and their hydrogenation into polyethylene-*block*-polystyrene-*block*-poly(ethylene oxide)s by sequential anionic polymerization is presented. The morphology of the triblock terpolymers was studied by means of transmission electron microscopy (TEM) and small-angle X-ray scattering (SAXS). The thermal properties were determined by standard differential scanning calorimetry (DSC) measurements. The values corresponding to the PEO block are here reported as a function of the volume fraction of the block in the terpolymer and the corresponding molecular weight. In this way we are able to account for the effect of the morphology in terms of the volume fraction, but also in terms of the molecular weight, which is of particular importance on the crystallization. Meanwhile, the properties calculated for the PE block are presented as a function of the polymerization degree and the volume fraction of either the PE or the PEO block. The last variable was employed because the PEO block is driving the microphase separation during the sample preparation.

Experimental Part

Synthesis. Anionic polymerization was carried out using solvents and monomers purified according to procedures described elsewhere.[27,28] The synthesis of poly(1,4-butadiene)-*block*-polystyrene-*block*-poly(ethylene oxide) (PB-*b*-PS-*b*-PEO) triblock terpolymers was realized by sequential anionic polymerization of butadiene, styrene, and ethylene oxide in benzene at 60 °C for butadiene and 40 °C for styrene and ethylene oxide using *sec*-BuLi as initiator. Polymerization of ethylene oxide in the presence of a lithium counterion was accomplished by using the strong phosphazene base *t*-BuP_4 (Fluka, 1 M in hexane, Li^+:*t*-BuP_4 1:1).[8,29−33] The polymerization of ethylene oxide was completed after 3 days and terminated with a mixture of methanol/acetic acid (1/5: v/v) followed by precipitation in 2-propanol. In the notation employed here ($A_xB_yC_z^m$), subscripts denote the percentage mass fraction of each block component and superscripts indicate the overall number-averaged molecular weight M_n in kg/mol of the block copolymer.

Hydrogenation. The hydrogenation of the PB-*b*-PS-*b*-PEO terpolymers (precursors) leads to PE-*b*-PS-*b*-PEO terpolymers.

* Corresponding author. E-mail: volker.abetz@gkss.de.
[†] GKSS Research Centre Geesthacht GmbH.
[‡] Universidad Simón Bolívar.

10.1021/ma0625713 CCC: $37.00
Published on Web 01/24/2007

Homogeneous catalytic hydrogenation was carried out with Wilkinson catalyst $(Ph_3P)_3Rh(I)Cl$ (Aldrich, 1 mol % with respect to the number of double bonds) in degassed toluene (1.53 wt % solution of the terpolymer) at 60 °C and 60 bar H_2 pressure for 3 days. ^1H NMR results of the hydrogenated terpolymers were used to confirm whether the PB block is completely hydrogenated. Further purification in order to eliminate residual Wilkinson catalyst was achieved by precipitation into 2-propanol followed by refluxing a toluene solution (0.7 wt % solution of the terpolymer) with a small amount of concentrated hydrochloric acid, again followed by precipitation into 2-propanol.

Size Exclusion Chromatography (SEC). SEC experiments of the polymer solutions in THF (2% w/v) were performed on a Waters instrument calibrated with narrowly distributed polybutadiene standards at 30 °C. Four PSS−SDV columns (5 μm, Polymer Standards Service, Mainz) with a porosity range from 10^2 to 10^5 Å were used together with a differential refractometer and a UV detector at 254 nm. Measurements on the non-hydrogenated triblock copolymers were performed in THF with a flow rate of 1 mL/min using toluene as internal standard.

Nuclear Magnetic Resonance Spectroscopy (^1H NMR). ^1H NMR spectra were recorded using a Bruker AC 250 spectrometer at 250 MHz. Non-hydrogenated samples were measured as solutions in $CDCl_3$ at room temperature, while hydrogenated samples were dissolved in d_8-toluene and measured at 40 °C. Solutions were prepared with 20 mg of the polymer in 0.8 mL of the corresponding solvent. Spectra were referenced to tetramethylsilane (TMS) as internal standard.

Transmission Electron Microscopy (TEM). The bulk morphology of PE-*b*-PS-*b*-PEO terpolymers and their corresponding precursors was studied by bright field TEM using a Zeiss CEM 902 electron microscope operated at 80 kV and a FEI Tecnai 20 operated at 200 kV. Films (around 0.5 mm thick) were prepared by casting from a 3 wt % solution of the terpolymer in toluene at 70 °C in order to avoid gelation upon solvent evaporation. After complete evaporation of the solvent (ca. 1 week), the films were slowly cooled to room temperature followed by drying under vacuum at room temperature for 1 day. Thin sections (thickness 50−100 nm) were cut at −130 °C using a Reichert-Jung Ultracut E microtome equipped with a diamond knife. In the hydrogenated terpolymers, staining of amorphous PEO and PS segments was accomplished by exposure of the thin sections to RuO_4 vapor for 30−40 min, which leads to a preferential staining of the PEO/PS microdomain interphase. The non-hydrogenated precursors were stained by exposure to OsO_4 vapor for 60 s, staining preferentially the PB block and the PS block to a smaller extent.

Small-Angle X-ray Scattering (SAXS). The material morphology was studied by means of temperature-dependent small-angle X-ray scattering (SAXS) at the A2 beamline of DORIS III, HASYLAB at DESY, Germany, using a temperature controlling system with liquid nitrogen as cooling fluid and 2D SAXS detector. The sample−detector distance was 3250 mm, and the wavelength was 1.5 Å. During the experiment, the sample was kept at 25 °C for 1 min to stabilize it, then heated up to 120 °C at 10 °C/min, kept 3 min at 120 °C in order to ensure complete melting, and cooled down to 25 °C at 10 °C/min. The SAXS diffraction patterns were recorded during the temperature program with 20 s frames starting every 30 s. Films cast as described in the previous section were used for the experiments.

Differential Scanning Calorimetry (DSC). A Perkin-Elmer PYRIS 1 differential scanning calorimeter in a dry nitrogen atmosphere with a CCA 7 liquid nitrogen cooling device was utilized. For all measurements a two-point calibration with *n*-decane and indium was carried out. Samples of 8 ± 0.5 mg were placed in the DSC pans. Standard heating and cooling scans were performed. The samples were heated up to 120 °C in order to exclude effects resulting from any previous thermal history, held at that temperature for 3 min, and then cooled down to −100 °C followed by the heating scan up to 120 °C. All experiments were carried out at a scanning rate of 10 °C/min. The shown cooling traces correspond to the first cooling, and the shown heating traces correspond to the following (second) heating scan. The degree of crystallinity for the PEO blocks was established from the normalized heat of fusion, while the degree of crystallinity for the PE blocks was calculated from the normalized heat of crystallization due to the vicinity of the melting endotherms of both blocks.

Scheme 1. Sequential Anionic Polymerization of PB-*b*-PS-*b*-PEO

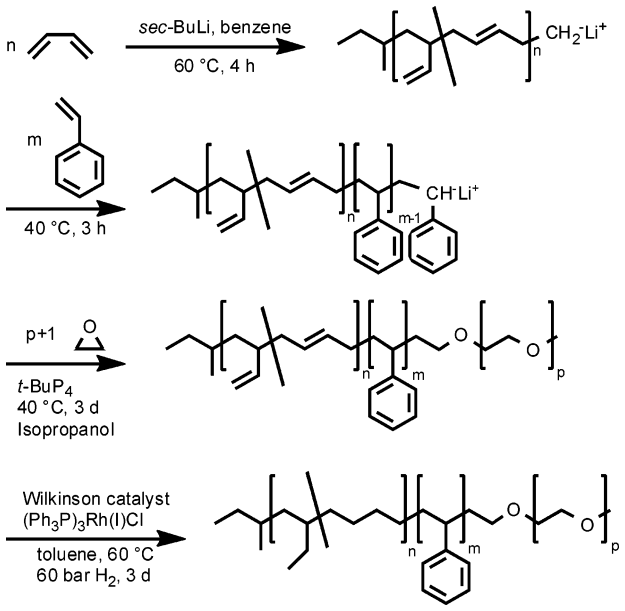

Results and Discussion

Synthesis. The PE-*b*-PS-*b*-PEO linear triblock terpolymers were prepared by homogeneous catalytic hydrogenation of the corresponding PB-*b*-PS-*b*-PEO linear triblock terpolymers. The synthesis of PB-*b*-PS-*b*-PEO terpolymers was accomplished by sequential anionic polymerization of butadiene, styrene, and ethylene oxide in benzene, as illustrated in Scheme 1. The polymerization of butadiene under the conditions employed leads to a preferential 1,4-addition (Table 1), which is essential in order to obtain the corresponding "high 1,4-hydrogenated PB" structure after hydrogenation, i.e., a random copolymer of ethylene and butene with a high ethylene content. Polymerization in a one-step procedure was achieved using the strong phosphazene base *t*-BuP_4,[8,29−33] allowing polymerization of ethylene oxide despite the presence of a Li^+ counterion.

SEC experiments (Figure 1) show that the reaction occurs without any significant termination, resulting in narrowly distributed PB-*b*-PS-*b*-PEO terpolymers (Table 1). Homogeneous catalytic hydrogenation was performed with a solution of the precursor triblock terpolymer in toluene using Wilkinson catalyst $(Ph_3P)_3Rh(I)Cl$ (Scheme 1). The hydrogenation efficiency under the experimental conditions was verified by ^1H NMR spectroscopy, showing a complete hydrogenation of the PB block (Figure 2).

Morphological Characterization. PB-*b*-PS-*b*-PEO and PE-*b*-PS-*b*-PEO terpolymers were analyzed by transmission electron microscopy (TEM) and small-angle X-ray scattering (SAXS) with the purpose of determining their morphology in bulk. In order to generate the contrast required for microscopy, the non-hydrogenated triblock terpolymers were stained with OsO_4 vapor, leading to a preferential staining of the PB block, while the hydrogenated triblock terpolymers were exposed to RuO_4 vapor, which favors the staining of the PEO/PS microdomain interphase. Figure 3 shows the TEM micrographs, and Figure 4 shows the SAXS patterns for the PB-*b*-PS-*b*-PEO and their

Table 1. Molecular Weight, Molecular Weight Distributions, and Content of 1,2-Units (wt %) in the Polybutadiene Block of the Triblock Terpolymers

	M_n (kg/mol)			
	PB[a] (%1,2[b])/PE[c]	PS[c]	PEO[c]	M_w/M_n
$B_{29}S_{40}EO_{31}^{168}/E_{29}S_{40}EO_{31}^{170}$	48 (12.9)/50	67	53	1.03
$B_{19}S_{34}EO_{47}^{142}/E_{19}S_{34}EO_{47}^{143}$	27 (12.8)/28	48	67	1.03
$B_{19}S_{35}EO_{46}^{217}/E_{19}S_{35}EO_{46}^{219}$	41 (10.8)/43	76	100	1.01
$B_{16}S_{68}EO_{16}^{210}/E_{17}S_{67}EO_{16}^{211}$	35 (11.5)/36	142	33	1.01
$B_{16}S_{40}EO_{44}^{143}/E_{16}S_{40}EO_{44}^{144}$	22 (14.0)/23	58	63	1.05
$B_{37}S_{16}EO_{47}^{76}/E_{38}S_{16}EO_{46}^{77}$	28 (11.8)/29	13	36	1.03

[a] Determined by SEC in THF calibrated against PB standards. [b] Determined by ^{1}H NMR spectroscopy in $CDCl_3$. [c] Determined by ^{1}H NMR spectroscopy using the molecular weight of the PB precursor obtained by SEC in THF calibrated against PB standards.

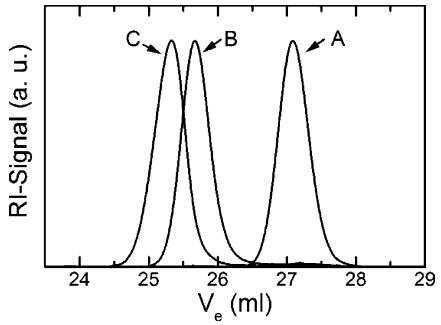

Figure 1. SEC traces of a synthesized PB-*b*-PS-*b*-PEO (C) linear triblock terpolymer including the PB (A) and PB-*b*-PS (B) precursors using THF as eluent, toluene as internal standard, and a Bischoff RI detector.

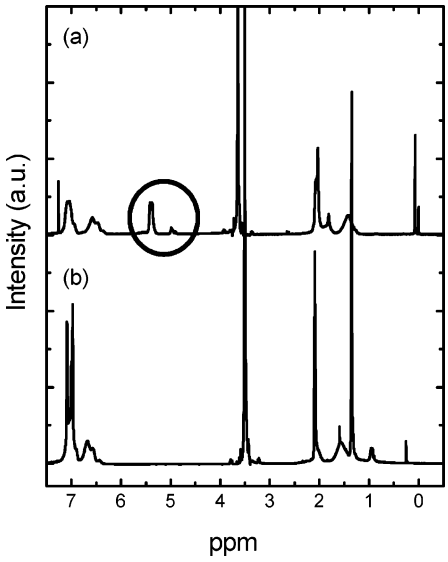

Figure 2. ^{1}H NMR spectra of a synthesized PB-*b*-PS-*b*-PEO (a) terpolymer and the corresponding PE-*b*-PS-*b*-PEO (b) terpolymer after hydrogenation with Wilkinson catalyst. Signals at $\delta = 5.8-5.4$ ppm corresponding to $-CH_2=$ bonds are presented in (a) (circled) but not in (b). Solvents employed were (a) $CDCl_3$, $\delta = 7.26$ ppm and (b) d_8-toluene, $\delta = 2.09$ ppm.

corresponding PE-*b*-PS-*b*-PEO triblock terpolymers (described in Table 1).

The micrographs presented in Figure 3 and the scattering patterns in Figure 4 evidence different morphologies for the synthesized triblock terpolymers according to their compositions. For the non-hydrogenated triblock terpolymers, fcc-packed spheres ($B_{16}S_{68}EO_{16}^{210}$, Figures 3a and 4a), connected hexagonally packed cylinders ($B_{29}S_{40}EO_{31}^{168}$, Figures 3c and 4c), and lamellar morphologies ($B_{16}S_{40}EO_{44}^{143}$, Figures 3e and 4e, $B_{19}S_{34}EO_{47}^{142}$, Figures 3g and 4g, $B_{19}S_{35}EO_{46}^{217}$, Figure 3i and no SAXS pattern, and $B_{37}S_{16}EO_{47}^{76}$, Figures 3k and 4i) are observed. The morphologies are formed by a compromise between PEO block crystallization and the interaction among the blocks (the segmental interaction parameters χ are listed in Table 2). With PEO being the less soluble block in the common solvent (i.e., toluene) and the only crystallizable block, it is expected to separate from the solution a lot earlier than PB or PS blocks, considering also that the PB/PS interaction parameter is the lowest among the three blocks. Therefore, the generated morphology will correspond to the one expected from a diblock, with a PEO block composition as in these triblocks. This may explain why four triblock terpolymers with different compositions but similar PEO block content (between 44 and 47 wt %) show all a lamellar morphology. It should be noted that the behavior depends on the solvent quality. Further annealing of the samples for times longer than 6 h or temperatures higher than 120 °C lead to more perfect structures, but did not change the morphology. It was not possible to determine whether those were equilibrium states, what was partially due to the high molecular weight of the terpolymers.

The SAXS patterns displayed in Figure 4 show better defined reflections in the molten state, meaning that the crystallization does affect the ordering of the microphases. However, most of the differences are in intensity, and only slight shifts in q values were observed in some of the cases. Mostly no real order−disorder or order−order phase transitions were observed upon cooling from the molten structure.

From the results shown in Figures 3 and 4 it is evident that the overall morphology of the non-hydrogenated triblock terpolymer is preserved in the corresponding hydrogenated triblock terpolymer after the hydrogenation procedures. The dimensions calculated from the patterns are presented in Table 3. Since in some cases the reflections are not well distinguished at 0 °C, the dimensions corresponding to the molten state are presented. It is worth noticing that the listed dimensions (i.e., lamellar spacing, sphere diameter) display differences mainly due to the presence of a second crystallizable block (hydrogenated PB or PE) which introduces restrictions and stresses to the microphase formation. Initially, two effects were expected. If crystallization occurs within the microphase, this will generate volume constrictions inside the given microphase due to increase in density. On the other hand, if crystallization breaks out or disrupts the microphase separation, then the crystals could dictate the morphology. The results here presented point toward the first situation. An example is given by the fact that the lamellar spacing of the lamellae-forming triblock terpolymers is always smaller after hydrogenation.

Very interesting exceptions of the above-mentioned tendency are the morphologies of $B_{16}S_{68}EO_{16}^{210}$ and $E_{17}S_{67}EO_{16}^{211}$ triblock terpolymers as well as those corresponding to the pair of $B_{16}S_{40}EO_{44}^{143}$ and $E_{16}S_{40}EO_{44}^{144}$. In the case of $B_{16}S_{68}EO_{16}^{210}$ and $E_{17}S_{67}EO_{16}^{211}$, due to the low content of both end blocks, in the non-hydrogenated triblock the resulting morphology is a typical cubic fcc array of PB (black) and PEO (white) spheres

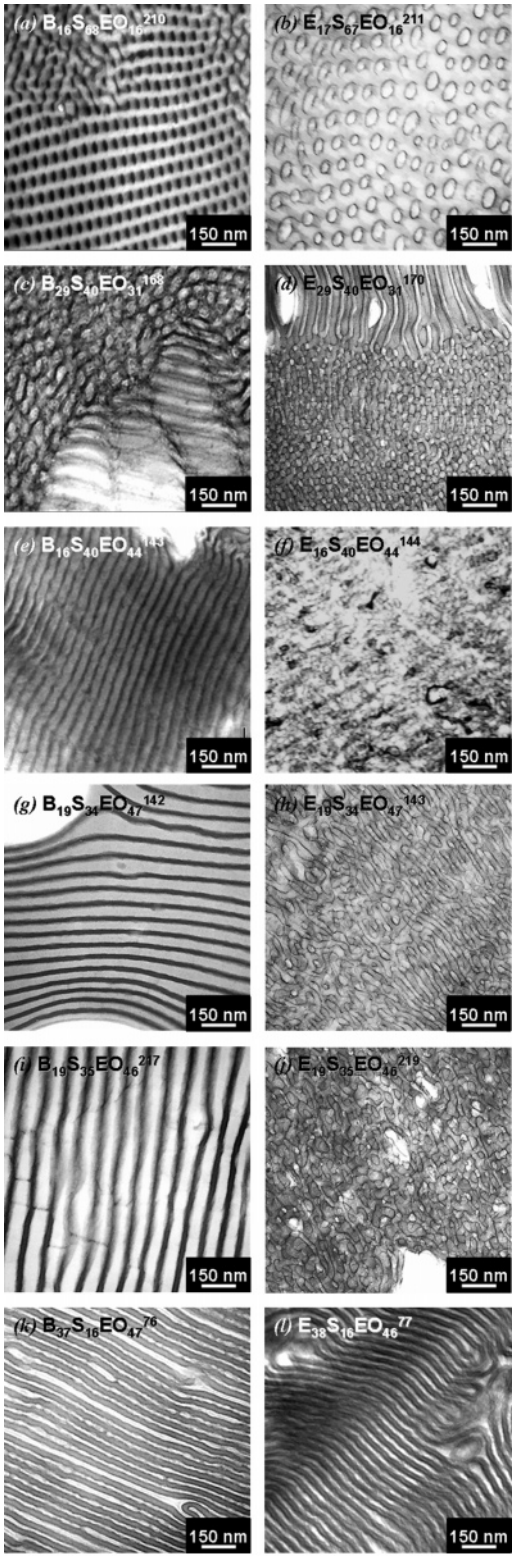

Figure 3. TEM micrograph for PB-*b*-PS-*b*-PEO (OsO_4 stained) and PE-*b*-PS-*b*-PEO (RuO_4 stained) triblock terpolymers. Ultrathin sections were obtained from films cast from toluene solutions at 70 °C. (a) $B_{16}S_{68}EO_{16}^{210}$, (b) $E_{17}S_{67}EO_{16}^{211}$, (c) $B_{29}S_{40}EO_{31}^{168}$, (d) $E_{29}S_{40}EO_{31}^{170}$, (e) $B_{16}S_{40}EO_{44}^{143}$, (f) $E_{16}S_{40}EO_{44}^{144}$, (g) $B_{19}S_{34}EO_{47}^{142}$, (h) $E_{19}S_{34}EO_{47}^{143}$, (i) $B_{19}S_{35}EO_{46}^{217}$, (j) $E_{19}S_{35}EO_{46}^{219}$, (k) $B_{37}S_{16}EO_{47}^{76}$, (l) $E_{38}S_{16}EO_{46}^{77}$.

(reflections at q^*, $1.6q^*$, $2q^*$). However, in the hydrogenated $E_{17}S_{67}EO_{16}^{211}$ we observed only one kind of PEO- or PE-containing sphere without a long-range order. Detailed work involving atomic force microscopy (AFM) measurements in order to investigate this particular case is the topic of a forthcoming contribution.

The difference in morphology after hydrogenation of $B_{16}S_{40}EO_{44}^{143}$ is given by the slight increase in interaction parameter of the PE block with the other two blocks and its crystallization ability. We assume that the PEO is the first block separating from the solution, since it is the block with the lowest solublity in toluene in the non-hydrogenated terpolymer, and the resultant morphologies do not vary significantly by hydrogenating the triblock terpolymer. After the PEO phase separation takes place, the PE is the first block to crystallize due to the set temperature for the film formation (none of the PEO blocks crystallizes above 70 °C, as will be presented later in Figures 7 and 8a). For this particular case, the crystallized PE cannot keep the lamellar morphology generated by the PEO block and causes a transformation of the PEO domains to cylinders. The PE domains could be distributed along the PS matrix forming a continuous phase, according to the TEM micrograph (Figure 3f). This fact points toward the possibility of disrupting the microphase separation by the PE crystallization under given conditions. Here we have only analyzed the morphologies after crystallization at 10 °C/min. The behavior could be affected when faster crystallization kinetics occurs, i.e., under quenching from the molten state.

Differential Scanning Calorimetry (DSC). In order to analyze and properly compare the thermal behavior of the triblock terpolymers, the projection of a 3D plot using the volume fraction ϕ and the polymerization degree N as the x and y axes will be used for the sake of comparison. In this way, it is possible to appreciate the influence of the volume fraction independently of the molecular weight and vice versa. The corresponding values of volume fraction ϕ and the polymerization degree N are presented in Table 4.

All the standard scans (shown in Figures 5 and 6) were performed at 10 °C/min, after melting the sample at 120 °C in order to erase any previous thermal history. Figure 7 shows the crystallization temperatures T_c, the melting temperatures T_m, and crystallinity α_c of the PEO block in the non-hydrogenated triblock terpolymers (PB-*b*-PS-*b*-PEO) as a function of the volume fraction ϕ and the polymerization degree N.

Most of the triblock terpolymers presented two crystallization peaks corresponding to the PEO block. The low-temperature exotherm was usually small and in several cases cannot be seen in Figure 5 in view of the scale employed to show all traces but was clearly visible upon scale magnification. These values are plotted in Figure 7 with the subscripts 1 and 2, corresponding to the low and high crystallization temperature, respectively. The subscripts are maintained even when one of the two peaks is not evident. This behavior is characteristic for fractionated crystallization and its origin is related to the difficulties that dispersed isolated phases encounter when the number of potentially crystallizing microdomains is orders of magnitude larger than the number of highly active heterogeneities in the system (more details of this well-known behavior can be found in refs 13 and 37). In this case, the high-temperature exotherm of the PEO block is due to the crystallization of microdomains that contain highly active heterogeneities and are probably connected with one another. The low-temperature exotherm corresponds to the crystallization of strictly isolated microdomains that either nucleate homogeneously (because they do not have any nucleating heterogeneity) or superficially and therefore need extreme supercoolings to crystallize (i.e., close to the T_g of the PEO block). The homogeneous nucleation of PEO nanospheres within block copolymers leads to peak crystallization temperatures (when cooled from the melt at 10 °C/min) of approximately −45 to −35 °C, while that of

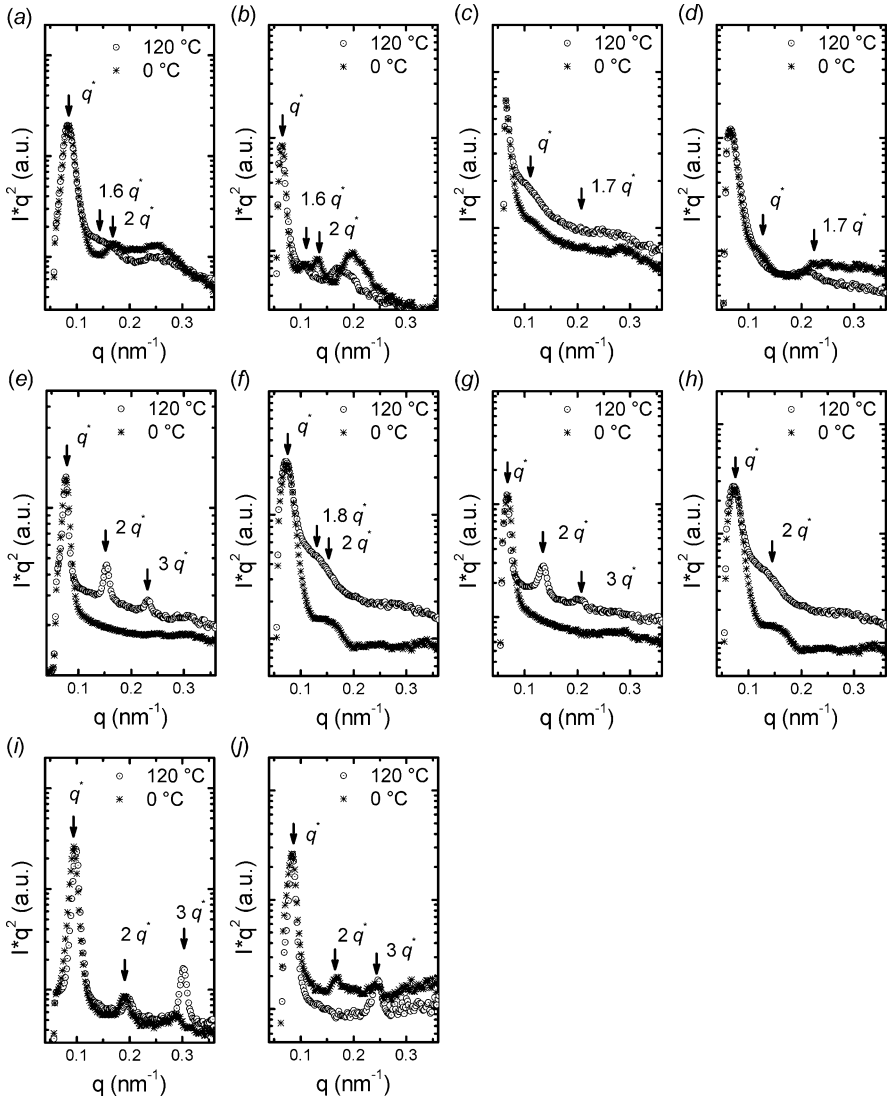

Figure 4. SAXS patterns for PB-*b*-PS-*b*-PEO and PE-*b*-PS-*b*-PEO triblock terpolymers at the molten state (120 °C) and after cooling down at 10 °C/min to 0 °C. Films cast from toluene solutions at 70 °C. (a) $B_{16}S_{68}EO_{16}^{210}$, (b) $E_{17}S_{67}EO_{16}^{211}$, (c) $B_{29}S_{40}EO_{31}^{168}$, (d) $E_{29}S_{40}EO_{31}^{170}$, (e) $B_{16}S_{40}EO_{44}^{143}$, (f) $E_{16}S_{40}EO_{44}^{144}$, (g) $B_{19}S_{34}EO_{47}^{142}$, (h) $E_{19}S_{34}EO_{47}^{143}$, (i) $B_{37}S_{16}EO_{47}^{76}$, (j) $E_{38}S_{16}EO_{46}^{77}$.

Table 2. Flory−Huggins−Staverman Enthalpic Segmental Interaction Parameters, Calculated at Different Temperatures[a]

	T (°C)		
	25	60	120
$\chi_{PB/PS}$	0.047	0.042	0.036
$\chi_{PE/PS}$	0.096	0.086	0.073
$\chi_{PB/PEO}$	0.14	0.12	0.10
$\chi_{PE/PEO}$	0.17	0.16	0.13
$\chi_{PS/PEO}$	0.052	0.046	0.039

[a] According to $\chi = (v/RT)(\delta_i - \delta_j)^2$, where v is the geometric average of the molar segmental volume calculated from the densities at room temperature (densities of the semicrystalline polymer were employed, using the corresponding crystallinity degrees calculated by DSC, and crystalline and amorphous values were taken from the literature ($\rho_{PB} = 0.9$ kg/m^3, $\rho_{PS} = 1.05$ kg/m^3; $\rho_{am-PE} = 0.887$ kg/m^3; $\rho_{cr-PE} = 0.999$ kg/m^3; $\rho_{am-PEO} = 1.123$ kg/m^3; $\rho_{cr-PEO} = 1.227$ kg/m^3),[34] density corrections for the real temperature are neglected). *RT* is the molar thermal energy at the given temperature.[35,36] The solubility parameters δ were taken from the literature.[34,36]

Table 3. Periodic Distances (*l*) and Diameters (*D*) of the Microphases Formed by the Triblock Terpolymers, Determined from the SAXS Patterns at 120 °C

non-hydrogenated terpolymers	hydrogenated terpolymers	{*hkl*}	*l* (nm)	*D* (nm)
$B_{16}S_{68}EO_{16}^{210}$		111	75	25
	$E_{17}S_{67}EO_{16}^{211}$	111	97	36
$B_{29}S_{40}EO_{31}^{168}$		100	59	
	$E_{29}S_{40}EO_{31}^{170}$	100	54	
$B_{16}S_{40}EO_{44}^{143}$		100	82	
	$E_{16}S_{40}EO_{44}^{144}$	100	87	
$B_{19}S_{34}EO_{47}^{142}$		100	94	
	$E_{19}S_{34}EO_{47}^{143}$	100	87	
$B_{37}S_{16}EO_{47}^{76}$		100	75	
	$E_{38}S_{16}EO_{46}^{77}$	100	66	

superficially nucleated droplets is speculated to occur at around −25 to −20 °C.[13,37]

In Figure 7 the values of T_{c1}, T_{c2}, T_m, and α_c for the PEO block within PB-*b*-PS-*b*-PEO are presented as a function of the block volume fraction, ϕ_{PEO}, and its polymerization degree, N_{PEO}. The plot of a projection of the thermal properties against these two values will allow the interpretation of the influence of block content independently from molecular weight. The effect of molecular weight on thermal transitions is well-known, but the effect of the volume fraction is more complicated since it indicates the influence of the microphase geometry on crystallization. Usually, it is expected that the thermal properties, i.e., T_c, T_m, and α_c, increase with the polymerization degree.[38] Additionally, it has been observed that the properties also increase with the volume fraction in block copolymers when the molecular weight of the block is constant.[11] These tendencies

Table 4. Volume Fraction ϕ^a of the PEO and PE Blocks within the Triblock Terpolymers, as Well as the Polymerization Degree, *N*, of the Corresponding Block

non-hydrogenated terpolymers	hydrogenated terpolymers	ϕ_{PEO}	N_{PEO}	ϕ_{PE}	N_{PE}
$B_{16}S_{68}EO_{16}^{210}$		0.14	743		
	$E_{17}S_{67}EO_{16}^{211}$	0.14	743	0.19	643
$B_{29}S_{40}EO_{31}^{168}$		0.27	1196		
	$E_{29}S_{40}EO_{31}^{170}$	0.27	1196	0.34	887
$B_{37}S_{16}EO_{47}^{76}$		0.41	808		
	$E_{38}S_{16}EO_{46}^{77}$	0.40	808	0.43	523
$B_{16}S_{40}EO_{44}^{143}$		0.40	1440		
	$E_{16}S_{40}EO_{44}^{144}$	0.40	1440	0.19	413
$B_{19}S_{34}EO_{47}^{142}$		0.43	1521		
	$E_{19}S_{34}EO_{47}^{143}$	0.42	1521	0.23	503
$B_{19}S_{35}EO_{46}^{217}$		0.41	2268		
	$E_{19}S_{35}EO_{46}^{219}$	0.41	2268	0.23	765

[a] Determined assuming additive volumes. Densities of the semicrystalline polymer were employed, using the corresponding crystallinity degrees calculated by DSC, and crystalline and amorphous values taken from the literature ($\rho_{PB} = 0.9$ kg/m^3, $\rho_{PS} = 1.05$ kg/m^3; $\rho_{am-PE} = 0.887$ kg/m^3; $\rho_{cr-PE} = 0.999$ kg/m^3; $\rho_{am-PEO} = 1.123$ kg/m^3; $\rho_{cr-PEO} = 1.227$ kg/m^3).[34]

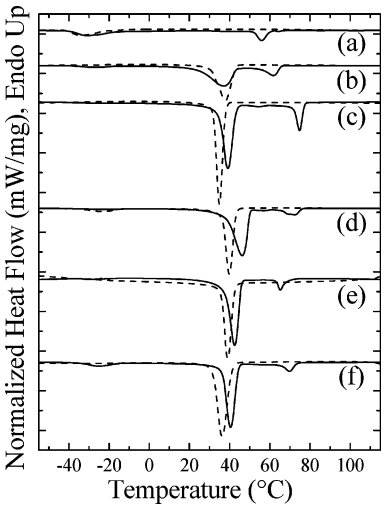

Figure 5. Standard DSC cooling traces recorded at 10 °C/min for the triblock terpolymers. The dashed traces correspond to the non-hydrogenated triblock terpolymers, and the continuous traces correspond to the hydrogenated ones. (a) $B_{16}S_{68}EO_{16}^{210}$ and $E_{17}S_{67}EO_{16}^{211}$, (b) $B_{29}S_{40}EO_{31}^{168}$ and $E_{29}S_{40}EO_{31}^{170}$, (c) $B_{37}S_{16}EO_{47}^{76}$ and $E_{38}S_{16}EO_{46}^{77}$, (d) $B_{16}S_{40}EO_{44}^{143}$ and $E_{16}S_{40}EO_{44}^{144}$, (e) $B_{19}S_{34}EO_{47}^{142}$ and $E_{19}S_{34}EO_{47}^{143}$, (f) $B_{19}S_{35}EO_{46}^{217}$ and $E_{19}S_{35}EO_{46}^{219}$.

are mostly shown by the presented results, as can be appreciated in Figure 7.

The values of crystallization temperature at low temperatures are presented in Figure 7a. Not all terpolymers presented a significant signal, since it will only occur when the PEO domain is isolated. It is peculiar that $B_{16}S_{40}EO_{44}^{143}$ ($\phi = 0.40$, $N = 1440$) shows the low-temperature crystallization and corresponds to a lamellar morphology. This fact reflects that connectivity among the lamellae is not high enough, and some of the material is therefore isolated, showing the effects of a homogeneous or superficial nucleation. Additionally, it could seem curious that $B_{19}S_{35}EO_{46}^{217}$ (0.41; 2268) showed a signal corresponding to T_{c1}, being the block with the higher volume fraction and molecular weight among the studied terpolymers. This could be related to the high molecular weight that implies a high segregation strength among the blocks. If this high segregation results in a low connectivity between the microphases, then the crystallization temperature could decrease significantly and even fractionate, as observed in this case. Note that the T_{c1} is lower for $B_{19}S_{35}EO_{46}^{217}$ than the one for $B_{16}S_{40}EO_{44}^{143}$ despite the molecular weight difference, indicating a higher amount of

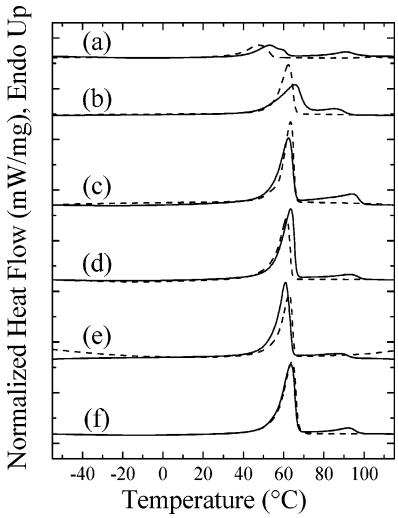

Figure 6. Standard DSC heating traces recorded at 10 °C/min for the triblock terpolymers. The dash traces correspond to the non-hydrogenated triblock terpolymers, and the continuous traces correspond to the hydrogenated ones. (a) $B_{16}S_{68}EO_{16}^{210}$ and $E_{17}S_{67}EO_{16}^{211}$, (b) $B_{29}S_{40}EO_{31}^{168}$ and $E_{29}S_{40}EO_{31}^{170}$, (c) $B_{37}S_{16}EO_{47}^{76}$ and $E_{38}S_{16}EO_{46}^{77}$, (d) $B_{16}S_{40}EO_{44}^{143}$ and $E_{16}S_{40}EO_{44}^{144}$, (e) $B_{19}S_{34}EO_{47}^{142}$ and $E_{19}S_{34}EO_{47}^{143}$, (f) $B_{19}S_{35}EO_{46}^{217}$ and $E_{19}S_{35}EO_{46}^{219}$.

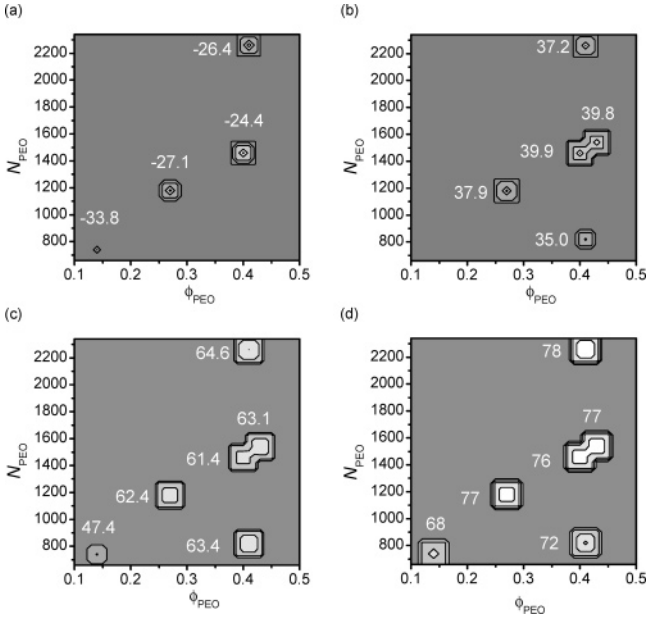

Figure 7. (a) T_{c1}, (b) T_{c2}, (c) T_m, and (d) α_c for the poly(ethylene oxide) block within the PB-*b*-PS-*b*-PEO triblock terpolymers as a function of ϕ_{PEO} and N_{PEO}. The color scale is lighter for higher values, and the numbers indicate the peak values. The crystallinity degree was calculated considering $\Delta H_{100\%} = 8.7$ kJ/mol[34] and normalizing the ΔH with the block weight.

isolated lamellae in the former triblock terpolymer. Additionally, it was already mentioned that the structures were not everywhere in the sample in the equilibrium state, and therefore a small fraction could form a structure other than lamellae. Because of its high molecular weight, it would be more difficult for $B_{19}S_{35}EO_{46}^{217}$ to achieve the equilibrium.

Figure 7b shows the crystallization temperature values at high temperatures, T_{c2}, corresponding to heterogeneous nucleation. The effect of the polymerization degree is stronger than the one of the volume fraction, as shown by $B_{29}S_{40}EO_{31}^{168}$ (0.27; 1196) having a higher T_{c2} than $B_{37}S_{16}EO_{47}^{76}$ (0.40; 808). The low T_{c2} value presented by $B_{19}S_{35}EO_{46}^{217}$ is due to the lack of connectivity discussed previously. There is no signal corresponding

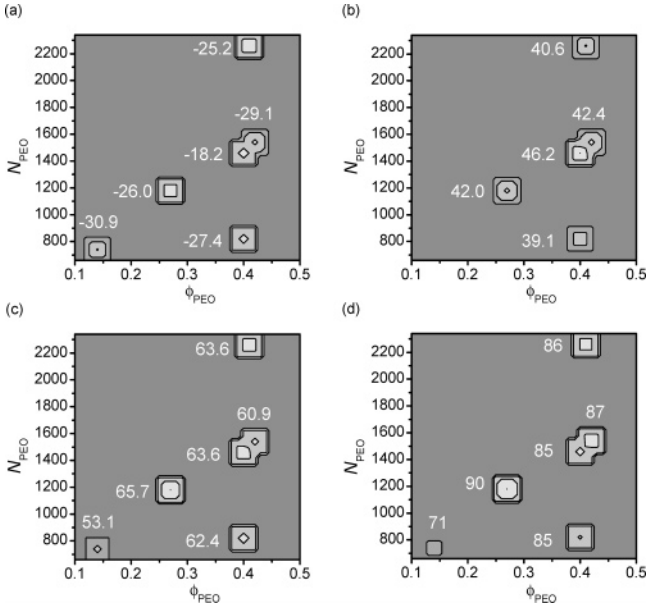

Figure 8. (a) T_{c1}, (b) T_{c2}, (c) T_m, and (d) α_c for the poly(ethylene oxide) block within the PE-*b*-PS-*b*-PEO triblock terpolymers as a function of ϕ_{PEO} and N_{PEO}. The color scale is lighter for higher values, and the numbers indicate the peak values. The crystallinity degree was calculated considering $\Delta H_{100\%} = 8.7$ kJ/mol[34] and normalizing the ΔH with the block weight.

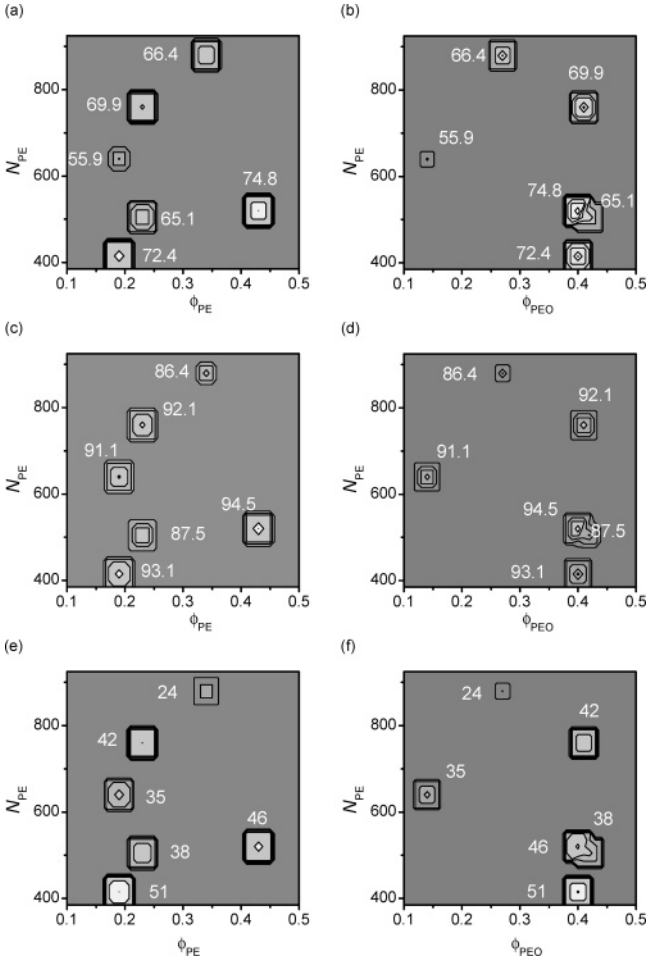

Figure 9. (a, b) T_c, (c, d) T_m, and (e, f) α_c for the polyethylene block within the PE-*b*-PS-*b*-PEO triblock terpolymers as a function of N_{PE} and (a, c, e) ϕ_{PE} or (b, d, f) ϕ_{PEO}. The color scale is lighter for higher values, and the numbers indicate the peak values. The crystallinity degree was calculated considering $\Delta H_{100\%} = 8.12$ kJ/mol[34] and normalizing the ΔH with the block weight.

to $B_{16}S_{68}EO_{16}^{210}$ (0.14; 743). This, together with its low value of peak crystallization temperature T_{c1}, indicates that most of the blocks are crystallizing from homogeneous nuclei generated within the isolated microdomains.[3−5,13,37,39,40]

The behavior corresponding to T_m is presented in Figure 7c. There is a marked difference between $B_{16}S_{68}EO_{16}^{210}$ and all the other terpolymers. The melting point is significantly lower when the material has crystallized in isolated domains exclusively. The corresponding values for the other terpolymers do not differ much, which is expected due to the crystal rearrangements that take place during heating. Finally, Figure 7d shows the variations in the crystallinity degree with N and ϕ for the PEO block. It is important to highlight that the percentage crystallinities derived from integrating enthalpies of DSC data have a large error because of baseline fluctuations and uncertainties in establishing the limits of integration. Therefore, the variations here observed should not be taken too rigorously within the associated error. However, one could say that α_c is observed to increase with both polymerization degree and volume fraction.

A representation of the thermal properties for the PEO block in the hydrogenated triblock terpolymers is presented in Figure 8. The crystallization temperature is presented for low temperatures, T_{c1} (Figure 8a), and high temperatures, T_{c2} (Figure 8b). The behavior of $E_{17}S_{67}EO_{16}^{211}$, $E_{29}S_{40}EO_{31}^{170}$, $E_{16}S_{40}EO_{44}^{144}$, and $E_{19}S_{35}EO_{46}^{219}$ for T_{c1} remains the same as it was before the hydrogenation (Figure 7a), mainly increasing with ϕ and N, with the particular case of $E_{19}S_{35}EO_{46}^{219}$ (0.41; 2268) being lower than $E_{16}S_{40}EO_{44}^{144}$ (0.40; 1440) due to a better segregation based on a higher molecular weight. However, new signals with low enthalpy changes appear for low-temperature crystallization of $E_{19}S_{34}EO_{47}^{143}$ (0.42; 1521) and $E_{38}S_{16}EO_{46}^{77}$ (0.40; 808), at very low T_{c1} values. This indicates that a very small population of PEO chains is crystallizing in isolated domains. Those domains have to be generated by the presence of either the PE block ($\chi_{PB/PEO}$ is slightly lower than $\chi_{PE/PEO}$, as reported in Table 2) or the PE crystals (physical constrains), since they were not evident on the non-hydrogenated terpolymers.

The high crystallization temperature T_{c2} shown in Figure 8b shows the same tendency as the corresponding non-hydrogenated terpolymers presented in Figure 7b and discussed previously. The polymerization degree has a greater influence than the volume fraction, the high molecular weight reflects high segregation strength and therefore isolated domains, and a very low volume fraction of PEO can lead to completely isolated domains that crystallize exclusively at low temperatures. Also, a similar behavior is shown by the melting temperature T_m (Figure 8c) and crystallinity degree α_c (Figure 8d), when compared to the corresponding results for PB-*b*-PS-*b*-PEO (Figures 7c and 7d, respectively).

On the basis of the evaluation of Figures 7 and 8, some comparison can be made in order to check the influence of the higher temperature crystallizable PE block on the thermal properties of the PEO block. In all cases it can be seen that the crystallization temperature T_{c2} of PEO increases after hydrogenation. A similar effect has been previously reported for PE-*b*-PEP-*b*-PEO, and it was attributed to the nucleating effect of some remaining Wilkinson catalyst;[3,13,37] a consistent increase in T_m and in the crystallinity degree can also be observed. This could also be a plausible explanation in the present case since it is known that it is very difficult to completely remove the impurities produced by adding this catalyst.[3]

The thermal properties of the PE block were plotted in Figure 9 as a function of the corresponding volume fraction (ϕ_{PE}), but

also as a function of the volume fraction of the PEO block (ϕ_{PEO}). The latter parameter turns out to be important since the PEO block is generally the first one that separates from the toluene solution and therefore templates the resulting morphology, as already discussed. Consequently, the PEO volume fraction is usually a better parameter for describing the overall morphology than the PE volume fraction itself.

The values of crystallization temperature T_c are presented in Figures 9a and 9b against ϕ_{PE} and ϕ_{PEO}, respectively. There is no recognizable tendency as a function of ϕ_{PE} (Figure 9a). However, T_c is observed to increase with the polymerization degree and the ϕ_{PEO} in Figure 9b. The effect of the PEO volume fraction on T_c is stronger than the one of the molecular weight, as described by the low T_c value of $E_{29}S_{40}EO_{31}^{170}$ ($\phi_{PEO} = 0.27$; $N_{PE} = 887$) despite the high molecular weight. There are two exceptions of the mentioned explanation. The first one is given by $E_{38}S_{16}EO_{46}^{77}$ ($\phi_{PE} = 0.43$; $\phi_{PEO} = 0.40$; $N_{PE} = 523$), which showed the highest T_c value despite its comparatively low polymerization degree. The reason could be related to the high PE content, which is the highest among the studied group. This could imply that there is a threshold in ϕ_{PE}, above which the crystallization temperature is much higher than the one for polymers with a similar ϕ_{PEO} but lower ϕ_{PE}. The second exception is $E_{16}S_{40}EO_{44}^{144}$ ($\phi_{PE} = 0.19$; $\phi_{PEO} = 0.40$; $N_{PE} = 413$), which has a high value of T_c for its low molecular weight and a low PE volume fraction. This is the only terpolymer where the PEO is not completely governing the microphase formation, and a contribution of the PE block distorts the original lamellae to generate PEO cylinders and a distributed PE phase in a PS matrix, as discussed before. The continuity of the PE phase is not described by any of the parameters employed in order to reflect the morphology, i.e., ϕ_{PEO} nor ϕ_{PE}, and continuous phases tend to have thermal properties similar to those corresponding to homopolymers, overcoming the restrictions imposed by the defined microphases.

The former situation is mostly repeated in Figures 9c and 9d for the melting temperature T_m. As for T_c, there is no obvious tendency when the variable is plotted as a function of ϕ_{PE}. The melting temperature increases with ϕ_{PE} and, more evidently, with ϕ_{PEO}. The case of $E_{38}S_{16}EO_{46}^{77}$ is an exception probably due to the high ϕ_{PE}, while the high value for $E_{16}S_{40}EO_{44}^{144}$ is due to the continuity of its PE phase. The melting temperature is also relatively high for $E_{17}S_{67}EO_{16}^{211}$ ($\phi_{PEO} = 0.14$; $N_{PE} = 643$), given the low crystallization temperature and low volume fractions of both PE and PEO blocks. In this case, the PE block probably undergoes massive reorganization during the heating scan since the originally generated lamellae should be very thin (as expected from the fact that the PE block here exhibits the lowest crystallization temperature as compared to other samples; this may be associated with homogeneous or superficial nucleation).[11,13] This is in good agreement with the broad melting peak observed in the DSC traces (Figure 6a). Even though the PEO block within this terpolymer crystallizes under similar conditions, the recrystallization and annealing of the PEO crystals take place to a lower extent than in the PE crystals. The high chain mobility and crystallization ability of the PE have been well studied.[41]

Finally, Figures 9e and 9f show the tendency of the crystallinity degree with the volume fractions and the molecular weight. The results agree with the previously observed trend of increasing with N and ϕ_{PEO}, showing a higher value than the expected for $E_{38}S_{16}EO_{46}^{77}$ attributed to the high ϕ_{PE} and for $E_{16}S_{40}EO_{44}^{144}$ because the PE phase is distributed along the matrix instead of being confined in a domain. Also, a higher than expected value of α_c for $E_{17}S_{67}EO_{16}^{211}$ was observed, probably caused by recrystallization upon heating.

Conclusions

The synthesis of novel poly(1,4-butadiene)-*block*-polystyrene-*block*-poly(ethylene oxide) (PB-*b*-PS-*b*-PEO) triblock terpolymers was successfully achieved by sequential anionic polymerization. Further hydrogenation of the high 1,4-PB block was also accomplished, obtaining triblock terpolymers with two crystallizable blocks. The morphology of the triblock terpolymers is determined by a compromise between crystallization of the polyethylene block and the segregation of the poly(ethylene oxide) block from the residual system. The observed morphologies from non-hydrogenated and hydrogenated triblock terpolymers indicate a sequential microphase separation where a template influence of the poly(ethylene oxide) domain prevailed. The effect was observed although the polyethylene block was the only one able to crystallize at the given film preparation conditions. However, because of the lower solubility of PEO, it microphase separates first and thus controls the overall formed morphology. The projection of a 3D plot of the thermal properties such as T_c, T_m, and α_c of the PE and PEO blocks against volume fraction and polymerization degree was successfully used to describe the dependence on domain geometry and molecular weight. A marked tendency of the PE block thermal properties with the PEO volume fraction was found, confirming that the PEO block templates the morphology and that the thermal properties are highly influenced by the morphology when the crystallization occurs inside the microphases. Some very interesting results were found, such as low crystallization temperature values for blocks with high molecular weights due to high segregation strength.

Acknowledgment. The authors thank their colleagues at Macromolecular Chemistry II of Bayreuth University for their collaboration. Special thanks to A. Göldel (Bayreuth University) and C. Abetz (GKSS Research Centre) for the TEM micrographs, Dr. H. Schmalz (Bayreuth University) for help during synthesis, and S. S. Funari (HASYLAB at DESY), D. Fierro (GKSS Research Centre), and J. Albuerne (GKSS Research Centre) for support with X-ray scattering. Financial support was given in part by Deutsche Forschungsgemeinschaft, HASYLAB and DESY.

References and Notes

(1) Hamley, I. W. *The Physics of Block Copolymers*, 1st ed.; Oxford: New York, 1998.
(2) Loo, Y. L.; Register, R. A. In *Developments in Block Copolymer Science and Technology*; Hamley, I. W., Ed.; Wiley: New York, 2004; p 213.
(3) Schmalz, H.; Knoll, A.; Müller, A. J.; Abetz, V. *Macromolecules* **2002**, *35*, 10004−10013.
(4) Chen, H.-L.; Li, H.-C.; Huang, Y.-Y.; Chiu, F.-C. *Macromolecules* **2002**, *35*, 2417−2422.
(5) Huang, Y.-Y.; Yang, C. H.; Chen, H.-L.; Chiu, F.-C.; Lin, T.-L.; Liou, W. *Macromolecules* **2004**, *37*, 486−493.
(6) Reiter, G.; Castelein, G.; Sommer, J.-U. In *Polymer Crystallization: Observations, Concepts and Interpretations;* Reiter, G., Sommer, J.-U., Eds.; Springer: Berlin, 2003; p 196.
(7) Zhu, L.; Huang, P.; Chen, W. Y.; Ge, Q.; Quirk, R. P.; Cheng, S. Z. D.; Thomas, E. L.; Lotz, B.; Hsiao, B. S.; Yeh, F.; Liu, L. *Macromolecules* **2002**, *35*, 3553−3562.
(8) Zhu, L.; Cheng, S. Z. D.; Calhoun, B. H.; Ge, Q.; Quirk, R. P.; Thomas, E. L.; Hsiao, B. S.; Yeh, F.; Lotz, B. *Polymer* **2001**, *42*, 5829−5839.
(9) Zhu, L.; Chen, Y.; Zhang, A.; Calhoun, B. H.; Chun, M.; Quirk, R. P.; Cheng, S. Z. D.; Hsiao, B. S.; Yeh, F.; Hashimoto, T. *Phys. Rev. B* **1999**, *60*, 10022−10031.
(10) Cohen, R. E.; Cheng, P.-L.; Douzinas, K.; Kofinas, P.; Berney, C. V. *Macromolecules* **1990**, *23*, 324−327.

(11) Lorenzo, A. T.; Arnal, M. L.; Müller, A. J.; Boschetti-de-Fierro, A.; Abetz, V. *Eur. Polym. J.* **2006**, *42*, 516−533.
(12) Takeshita, H.; Ishii, N.; Araki, C.; Miya, M.; Takenaka, K.; Shiomi, T. *J. Polym. Sci., Part B: Polym. Phys.* **2004**, *42*, 4199−4206.
(13) Müller, A. J.; Balsamo, V.; Arnal, M. L. *Adv. Polym. Sci.* **2005**, *190*, 1−63.
(14) Fluodas, G.; Reiter, G.; Lambert, O.; Dumas, P. *Macromolecules* **1998**, *31*, 7279−7290.
(15) Jiang, S.; Chaoliang, H.; An, L.; Chen, X.; Jiang, B. *Macromol. Chem. Phys.* **2004**, *205*, 2229−2234.
(16) Albuerne, J.; Márquez, L.; Müller, A. J.; Raquez, J. M.; Degée, P.; Dubois, P.; Castelleto, V.; Hamley, I. W. *Macromolecules* **2003**, *36*, 1633−1644.
(17) Müller, A. J.; Albuerne, J.; Esteves, L. M.; Márquez, L.; Raquez, J. M.; Degée, P.; Dubois, P.; Collins, S.; Hamley, I. W. *Macromol. Symp.* **2004**, *215*, 369−382.
(18) Müller, A. J.; Albuerne, J.; Márquez, L.; Raquez, J.-M.; Degée, P.; Dubois, P.; Hobbs, J.; Hamley, I. W. *Faraday Discuss.* **2005**, *128*, 231−252.
(19) Sun, L.; Liu, Y.; Zhu, L.; Hsiao, B. S.; Avila-Orta, C. A. *Polymer* **2004**, *45*, 8181−8193.
(20) Hamley, I. W.; Castelletto, V.; Castillo, R. V.; Müller, A. J.; Martin, C. M.; Pollet, E.; Dubois, P. *Macromolecules* **2005**, *38*, 463−472.
(21) Hamley, I. W.; Parras, P.; Castelletto, V.; Castillo, R. V.; Müller, A. J.; Pollet, E.; Dubois, P.; Martin, C. M. *Macromol. Chem. Phys.* **2006**, *207*, 941−953.
(22) Arnal, M. L.; Balsamo, V.; López-Carrasquero, F.; Contreras, J.; Carrillo, M.; Schmalz, H.; Abetz, V.; Laredo, E.; Müller, A. J. *Macromolecules* **2001**, *34*, 7973−7982.
(23) Balsamo, V.; Von Gyldenfeldt, F.; Stadler, R. *Macromol. Chem. Phys.* **1996**, *197*, 3317−3341.
(24) Balsamo, V.; Müller, A. J.; von Gyldenfeldt, F.; Stadler, R. *Macromol. Chem. Phys.* **1998**, *199*, 1063−1072.
(25) Balsamo, V.; Müller, A. J.; Stadler, R. *Macromolecules* **1998**, *31*, 7756−7763.
(26) Müller, A. J.; Balsamo, V.; Arnal, M. L. In *Lecture Notes in Physics: Progress in Understanding of Polymer Crystallization*; Reiter, G., Strobl, G., Eds.; *Lect. Notes Phys.* **2007**, *714*, 229−259.
(27) Schmalz, H.; Abetz, V.; Lange, R.; Soliman, M. *Macromolecules* **2001**, *34*, 795−800.
(28) Schmalz, H.; Böker, A.; Lange, R.; Krausch, G.; Abetz, V. *Macromolecules* **2001**, *34*, 8720−8729.
(29) Esswein, B.; Molenberg, A.; Möller, M. *Macromol. Symp.* **1996**, *107*, 331−340.
(30) Esswein, B.; Möller, M. *Angew. Chem.* **1996**, *108*, 703−705.
(31) Esswein, B.; Steidl, N. M.; Möller, M. *Macromol. Rapid Commun.* **1996**, *17*, 143−148.
(32) Förster, S.; Krämer, E. *Macromolecules* **1999**, *32*, 2783−2785.
(33) Floudas, G.; Vazaiou, B.; Schipper, F.; Ulrich, R.; Wiesner, U.; Iatrou, H.; Hadjichristidis, N. *Macromolecules* **2001**, *34*, 2947−2957.
(34) Grulke, E. A. In *Polymer Handbook*, 4th ed.; Brandrup, J., Immergut, E. H., Grulke, E. A., Eds.; J. Wiley & Sons: New York, 1999; p VII/675.
(35) Stadler, R.; Auschra, C.; Beckmann, J.; Krapper, U.; Voigt-Martin, I.; Leibler, L. *Macromolecules* **1995**, *28*, 3080−3097.
(36) Barton, A. F. *CRC Handbook of Polymer Liquid Interaction Parameters and Solubility Parameters*; CRC Press: Boca Raton, FL, 1990; p 245.
(37) Müller, A. J.; Balsamo, V.; Arnal, M. L.; Jakob, T.; Schmalz, H.; Abetz, V. *Macromolecules* **2002**, *35*, 3048−3058.
(38) Evans, R. D. M.; Harold, R.; Flory, P. J. *J. Chem. Phys.* **1947**, *15*, 685.
(39) Massa, M. V.; Dalnoki-Veress, K. *Phys. Rev. Lett.* **2004**, *92*, 255509.
(40) Reiter, G.; Castelein, G.; Sommer, J. U.; Röttele, A.; Thurn-Albrecht T. *Phys. Rev. Lett.* **2001**, *87*, 226101.
(41) Organ, S. J.; Keller, A. *J. Polym. Sci., Part C: Polym. Lett.* **1987**, *25*, 67−72.

MA0625713